Influence of surface roughness on the elastic-light scattering patterns of micron-sized aerosol particles

**J.-C. Auger · G.E. Fernandes · K.B. Aptowicz ·
Y.-L. Pan · R.K. Chang**

Abstract The relation between the surface roughness of aerosol particles and the appearance of island-like features in their angle-resolved elastic-light scattering patterns is investigated both experimentally and with numerical simulation. Elastic scattering patterns of polystyrene spheres, *Bacillus subtilis* spores and cells, and NaCl crystals are measured and statistical properties of the island-like intensity features in their patterns are presented. The island-like features for each class of particle are found to be similar; however, principal-component analysis applied to extracted features is able to differentiate between some of the particle classes. Numerically calculated scattering patterns of Chebyshev particles and aggregates of spheres are analyzed and show qualitative agreement with experimental results.

1 Introduction

In recent years, two-dimensional angular optical scattering (TAOS) has been investigated as a potential tool for use in the detection and characterization of aerosols in the micrometer range [1–4]. Whereas several techniques have been able to measure TAOS patterns of micro-particles in real time, limited effort has been put into interpreting the information

contained in TAOS patterns. As a result, most particle detection and characterization systems in use today rely on alternative techniques, such as fluorescence spectroscopy, LIBS, or mass spectroscopy, for their smaller data sets that can be more readily analyzed with standard statistical procedures [5–7]. Here we study the relationship between the appearance of isolated peaks (islands formed by high scattered intensity) in the TAOS patterns and the surface roughness of the scattering particle. The particles considered here are aggregates of submicron- or micron-sized polystyrene spheres, *Bacillus subtilis* spores and cells, and NaCl crystals, with an approximate overall diameter of 8 μm. Using image processing techniques, we demonstrate that the density of islands is related to the surface roughness of the aggregates, although trends appear not to be monotonic. In addition, by using statistical information extracted from the island patterns, we are able to distinguish between the TAOS patterns of various different aggregates.

TAOS is an attractive technique for detecting and characterizing airborne particles for a number of reasons. First, TAOS patterns contain information on the particle's size, geometry, orientation, surface roughness, and refractive index [8]. Second, TAOS has a substantially larger cross-section compared with other techniques such as fluorescence or Raman spectroscopy, and thus minimizes the requirements for laser-source power and detector sensitivity. Third, TAOS systems can be assembled from laser diode sources and off-the-shelf CCD detectors, components which have reached high levels of technological maturity, and thus can be obtained at relatively low costs and in compact sizes. Finally, the TAOS technique does not require expendable components such as buffer solutions or the constant cleaning and alignment of parts, making it possible to build low-cost and high-efficiency TAOS systems that can be deployed and left to operate for extended periods of time with little mainte-

J.-C. Auger (✉) · G.E. Fernandes · R.K. Chang
Center for Laser Diagnostics and Department of Applied Physics,
Yale University, New Haven, CT 06520, USA
e-mail: augerjc@gmail.com

K.B. Aptowicz
Department of Physics, West Chester University, West Chester,
PA 19383, USA

Y.-L. Pan
U.S. Army Research Laboratory, Adelphi, MD 20783, USA

nance. It is therefore desirable to learn to interpret TAOS data in order to improve the usability of TAOS in particle detection and characterization systems. Although direct comparisons of experimentally measured TAOS patterns with numerically calculated TAOS patterns have been successfully performed [9], such exact comparisons are practically unfeasible for all but the simplest cases under controlled experiments, where much information about the scattering particle is known beforehand. Owing to the difficulty in interpreting TAOS patterns by direct comparison with numerical predictions, an indirect approach is generally required. The indirect approach consists of grouping TAOS patterns according to their common traits (e.g. mean intensity per pixel within an angular range, size and sphericity of the islands, degrees of symmetry, etc.) and statistically relating these traits to properties of the scattering particle.

Previous experimental studies of TAOS [1, 4, 10, 14] have shown that aggregates of particles produce patterns with large numbers of isolated higher intensity islands. Although no qualitative relationship was established between the properties of the islands in the TAOS pattern and those of the scattering aggregate of particles, island characteristics such as size, shape, spatial frequency, and intensity were observed to vary from pattern to pattern. In this study we use image processing techniques to demonstrate that larger surface roughness leads, in general, to larger numbers of islands per steradian in the TAOS patterns of homogeneous aggregates of particles. Using the method of principal-components analysis (PCA), TAOS patterns from polystyrene latex sphere aggregates and other substances including *Bacillus subtillis* (BG) cells and spores are sorted based on their island characteristics alone, and good distinction is achieved for a variety of aggregate types. Our findings are further supported with numerical T-Matrix simulations of aggregates of spheres, where the primary particles size is varied, and T-matrix simulations of single Chebyshev particles, where the amplitude and period of the perturbation are varied.

2 Experimental methods and results

We investigated a series of experimental TAOS patterns collected in the backward hemisphere ($90° < \theta < 168°$ and $0° < \phi < 360°$) for various homogeneous polystyrene latex sphere (PSL) aggregates. The details of the experimental setup are given in references [1, 2]. In this study, the number of spheres per aggregate was controlled by varying the concentration of PSL spheres in the solution placed in an inkjet aerosol generator (IJAG) [11]. The illuminating wavelength, 0.532 μm, was provided by a single 30 ns pulse from a frequency-doubled Nd:YAG laser (Spectra Physics, model X-30). The TAOS patterns from the backward hemisphere

were collected by an elliptical mirror and projected onto an image-intensified CCD detector, with 1024×1024 pixel resolution. In order to isolate the effects of surface roughness on the TAOS patterns, the overall radius of the aggregates was fixed at approximately 8 μm for all measurements, so that changes in the TAOS patterns were dominated by the effects of surface roughness changes caused by different sizes of the primary particles. PSL sphere diameters of 0.202, 0.988 and 2.9 μm were chosen as the primary sphere sizes for the aggregates. Other aggregates were formed from nonspherical primary particles for comparison, including *Bacillus subtilis* (BG) cells and BG spores, and NaCl crystals.

A Matlab based image analysis routine [2, 12] was applied to each TAOS pattern to obtain a black-and-white profile of the islands, as illustrated in Fig. 1(a). The black-and-white island profile was then used to calculate the size distribution of the islands. The following steps are involved in the image processing routine: (1) the background is removed from the TAOS pattern; (2) a spatial mean-filter is applied to the TAOS pattern to remove ICCD noise; (3) the pixel intensities are equalized by taking the square root of the pixel values; (4) the extended maxima (island peaks) and watershed lines of the filtered image are found; (5) minima are imposed on the gradient of the filtered image (found by applying a Sobel-type filter [12]) at the location of the island peaks and watershed lines found in step 4; (6) the watershed lines of the result of step 5 give the island contours. This procedure computes the regional maxima throughout the TAOS pattern, and thus is more accurate than simply applying a global intensity threshold to the smoothed image.

Step 4 above requires the specification of a threshold value for the computation of the extended maxima. The
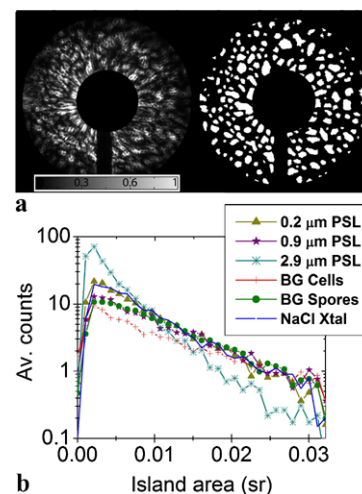
Fig. 1 (**a**) Backward hemisphere TAOS pattern (*left*) and the corresponding image processing routine output (*right*) from a single 8 micron particle aggregate formed by 0.98 micron PSL spheres. (**b**) Averaged island area histograms from TAOS patterns of different kinds of aggregates formed with different types of micron-sized particles

Table 1 Island counting routine results (data in bracket: standard deviation)

Primary particle	Mean number of islands per sr	Mean island area in sr	Mean island eccentricity
BG Cell	11 (5)	0.0103 (0.0007)	0.716 (0.026)
BG Spores	15 (3)	0.0098 (0.0003)	0.709 (0.022)
PSL Sphere (0.988 μm diameter)	16 (5)	0.0098 (0.0004)	0.714 (0.022)
NaCl Crystal	20 (6)	0.0088 (0.0012)	0.703 (0.014)
PSL Sphere (0.202 μm diameter)	21 (5)	0.0081 (0.0007)	0.723 (0.015)
PSL Sphere (2.900 μm diameter)	36 (6)	0.0047 (0.0010)	0.693 (0.015)

threshold is specified as a fixed fraction of the (regional) maximum intensity. Small variations of the threshold value did not significantly affect the results, which indicates that the filtering and equalization steps efficiently removed the high frequency oscillations caused by experimental noise. For the results presented here, the threshold value was kept constant at 0.5. Then, a standard Matlab routine was applied to the results of step 6 above to obtain the number and area (in pixels) of the islands. The results obtained for each TAOS pattern were then averaged over the entire data set (each data set consisted of different TAOS patterns obtained from different individual aggregates generated by the IJAG with the same concentration of the same primary submicron- or micron-sized particles), and the averages were plotted on a 30-bin histogram.

Figure 1(b) shows the island area histograms averaged over each data set. The histograms in Fig. 1(b) are seen to follow a log-normal distribution. We believe that this type of distribution is caused by the smaller islands that are identified by the routine, which are limited by the size of spatial filter used to remove pixel noise from the pattern. Thus, spatial filtering imposes a cutoff on the smaller island sizes. In order to achieve good results with the island counting routine, it is necessary to optimize the filter size together with the threshold value for the extended maxima discussed above. This was done visually, by comparing the output of the island outlining routine with the original TAOS patterns. We found that a filter size of ~10 pixels ~10^{-4} sr) provided the best results.

The mean number of islands, the mean island area, and the mean island eccentricity (i.e. the aspect ratio of the ellipse encompassing the particle) for the aggregates in Fig. 1(b) are listed in Table 1. It is interesting to notice that the values for BG spore aggregates are very similar to those for 0.988 μm PSL aggregates. Single BG spores are approximately 1 μm in length and 0.5 μm in width, thus having volume similar to the 0.988 μm PSL sphere. In particular, little difference is observed in the mean island eccentricity (which measures the amount of deviation in island shape relative to

a perfect circle) for all samples. One possible explanation for this result is the fact that, even though the BG spores are non-spherical, their orientation in the cluster of particles is random.

The island properties of TAOS patterns from different kinds of particle aggregates were used as input variables in a sorting routine based on the principal-components analysis (PCA) [13]. Thirty-two variables were chosen to represent each TAOS pattern, the first 30 being the values in each of the island area histogram bins, and the last two being the total number of islands in the histogram and the mean island eccentricity, respectively. The PCA results are plotted in Fig. 2 for various combinations of samples. The horizontal axis correspond to the first principal component, and the vertical axis correspond to the second principal component. The dashed lines in some of the plots are suggested boundaries between different samples. Fig. 2(a) shows the PCA results for all samples listed in Table 1. It can be seen that most of the variance in the data is accounted for by the first principal component. The second principal component helps improve the distinction between several types of aggregates, but the third principal component was not found to significantly contribute, and thus was omitted from this analysis.

In Fig. 2(b), the PCA method is seen to reliably distinguish between aggregates formed from three different sizes of PSL spheres based on the island properties alone. Good distinction was also achieved between the BG spore aggregates and the 0.2 and 2.9 μm PSL aggregates, Fig. 2(c). As expected from the similarity of their island area and eccentricity histograms (Fig. 1(b) and Table 1), the distinction between the BG spore aggregates and the 0.988 μm PSL aggregates was poor (see Fig. 2(e)). The distinction between 0.202 μm PSL spheres and NaCl crystal aggregates (Fig. 2(d)) was also poor. A similar PCA run was performed without the mean eccentricity, and yielded similar results. As can be seen in Table 1, the mean island eccentricity did not vary greatly between different samples. The results shown in Fig. 2 for the PCA routine suggest that distinction between samples can range from excellent to poor,
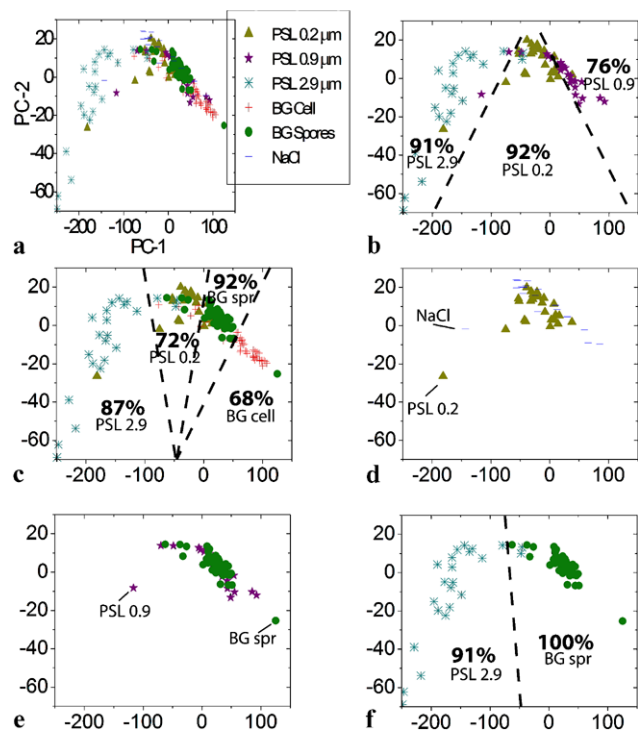
Fig. 2 (**a**) Results of the principal-component analysis (PCA) sorting routine applied to various combinations of aggregates formed from different primary submicron- or micron-sized particles. The dashed lines were included in the cases where some distinction is apparent to suggest the boundaries between different aggregates in the PCA plane. The percentages indicate the fraction of samples that fell within the boundaries. (**b**)–(**f**) are comparisons for different groups

depending on which samples were combined. PCA runs including the eccentricity histograms were also performed but did not provide significant improvements in the results.

3 Numerical simulations studies

To further develop the relationship between surface roughness of an aerosol particle and the island-like features in the TAOS pattern, we applied multiple scattering T-matrix theory (MTM) [17] to calculate TAOS patterns of dense clusters composed by randomly aggregated spherical particles. MTM allows for the intrinsic optical properties of the cluster to be calculated independently of the direction and polarization of the incident and scattered fields. Consequently, once a calculation is done for a particular particle, an infinite number of patterns can be generated with minimal effort, where each pattern represents a different illumination configuration.

Here we model aggregates of 13 and 45 PSL spheres with radii of 0.532 and 0.335 micrometers respectively. TAOS patterns are calculated in the full backward hemisphere ($\pi/2 \leq \theta \leq \pi$ and $0 \leq \phi \leq 2\pi$) with respect to the direction of the incident wave vector. The dimensions of the spheres

are chosen such that the total volume of the polymer in each aggregate is kept constant to simulate the experimental conditions. The wavelength of the incident linearly polarized plane wave is set to 0.532 μm. The index of refraction of the particles and the surrounding medium are $1.6 + 0.0i$ and $1.0 + 0.0i$ (vacuum) respectively. The image analysis routine applied to the calculated TAOS patterns is similar to that applied to the experimentally measured ones, except that the steps used to remove detector noise are omitted.

Figure 3 shows the island area histograms of 40 different TAOS patterns calculated from 10 randomly generated densely packed sphere clusters of primary particles with radii of (a) 0.532 μm and (b) 0.335 μm. Calculations were performed at two different random orientations and polarizations for each cluster. The numerical results indicate a similar trend to that observed in the experiments: that larger primary particles lead to a larger number of smaller islands in the TAOS pattern, as well as a shorter tail of the histogram.

A systematic study of the TAOS patterns as a function of the number and size of the primary particles involves unrealistic computational resources [16]. In addition, MTM cannot model the light scattering properties of compact clusters composed by non-spherical particles. Consequently, the study of aggregates of spores must be achieved using alternative techniques such as the Discrete Dipole Approximation (DDA) [15], which are also prohibitively time consuming. In order to work around such restrictions, we used the single scattering T-Matrix method (STM) to generate TAOS patterns from a series of Chebyshev particles [18]. The surface of a Chebyshev particle is given by $r(\theta) = r_0(1 + \zeta \cos n\theta)$, where r_0 is the radius of the unperturbed sphere, ζ is the deformation amplitude and n is the polynomial order. We used this simple model to investigate how changes in the surface roughness alone affect the properties of islands appearing in the TAOS patterns.

We assume that the presence of microvoids in aggregates of non-penetrable objects is not susceptible to significantly influence the structure of their TAOS pattern in terms of island sizes and numbers when compared to an homogeneous particle with identical surface morphology. Whether experimental confirmation of this hypothesis is practically impossible because of the difficulties to measure the numbers and size of the microvoids in the clusters, numerical studies via DDA or FDTD algorithms could bring more understanding. Nonetheless to our knowledge no systematic study has been performed yet on this topic.

The wave vector of the incident radiation was kept perpendicular to the axis of symmetry of the Chebyshev particle and the analyzed patterns were obtained after averaging over the two polarizations. In such conditions, as ζ vanishes or $n \gg 1$, the resulting TAOS patterns approach the well-known concentric ring structure of a spherical particle. Systematic calculations were performed in the ranges

Fig. 3 Island size histograms of the TAOS patterns calculated from dense aggregated spheres with different size of primary particles: (**a**) $r = 0.532$ μm, (**b**) $r = 0.335$ μm
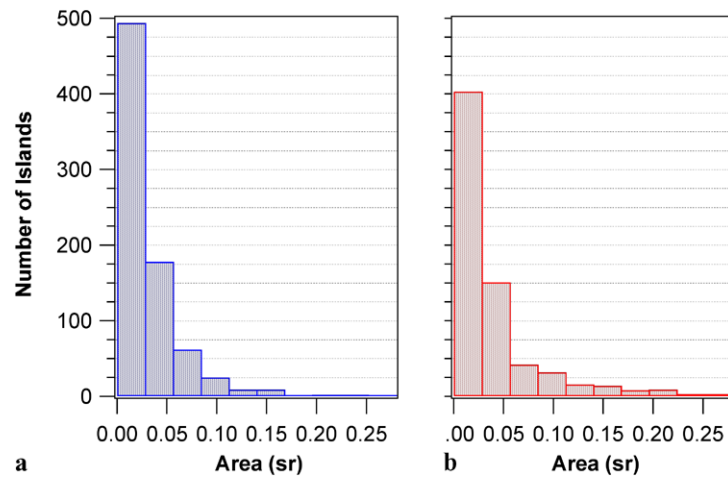

$1.0 \leq r_0 \leq 3.0$, $0.0 \leq \zeta \leq 0.3$ and $10 \leq n \leq 100$. The combined values of ζ and n were chosen to approximate the amplitude of the surface oscillations of realistic aggregates. Finally, the image analysis procedure performed on the TAOS patterns was simplified as follows: (a) the scattered intensities were normalized from 0 to 256; (b) a threshold was applied to obtain a black-and-white profile of the patterns; and (c) the surface area of each island encountered in the resulting image was calculated.

At very small surface roughness, the TAOS patterns showed the concentric ring structure expected for a sphere. The rings of highest intensity were found in the near backscattering direction. As the roughness increases with fixed r_0, the ring structure breaks down and the island-like intensity features appear throughout the TAOS pattern. The islands of highest intensity show no preference towards the near backscattering direction. Consequently, the number of islands captured in our image analysis increases and the mean island size decreases. This occurred independent of the threshold value set for image analysis, although variation in the threshold value did modify the total number of islands in each TAOS pattern.

An interesting feature is obtained when ζ is kept constant and n is increased. Under such conditions the number of islands decreases and their surface area increases with n, as expected, until n exceeds a certain value, n_{max}, above which the TAOS patterns remain practically unchanged. Furthermore, n_{max} is seen to increase with r_0. This trend confirms that not only the height of the surface oscillation is an important parameter, but also that its spatial extension can also influence the structure of the TAOS, as long as it is not too small in comparison to the wave length of the incident radiation.

Finally, in order to simulate large aggregates composed by primary objects having different sizes, with dimensions that could not be reached using MTM formalism, we constructed a series of Chebychev particles varying r_0 from 1.25
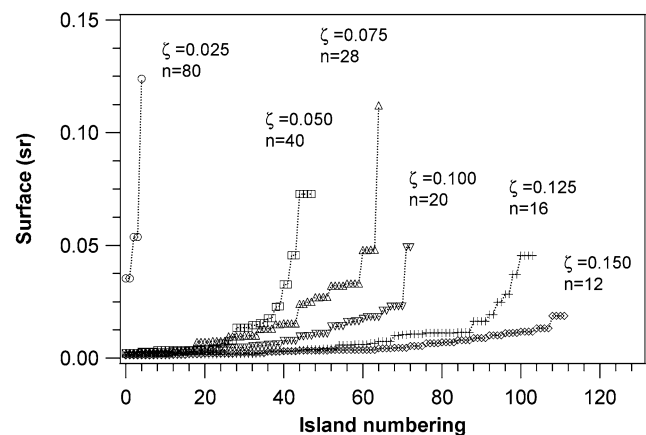
Fig. 4 Island analysis from the TAOS patterns of various Chebyshev particles setting r_0 to 2.5 μm and varying ζ and n (see the figure for details). The x-axis represents the numbering of each island in each TAOS. The total number of islands ranges from 5 ($\zeta = 0.025$, $n = 80$) to 112 ($\zeta = 0.150$, $n = 12$)

to 3.0 micrometers. ζ and n were modulated simultaneously such that $\zeta = r_p/2$, and $n = 2\pi r_0/4r_p$, where r_p represents the equivalent radius of the primary particles. Typical results shown in Fig. 4, for $r_0 = 2.5$ micrometers, clarify the relationship between the deformation parameters and the resulting island properties. As expected, large deformation parameters combined with a small number of surface oscillations are seen to lead to larger number of islands with small island areas. Also, if this trend was generally observed, it happened that for some combination of r_0 and n, intermediary values of ζ could lead to a decrease in the number of islands.

4 Summary

The task of interpreting TAOS patterns in terms of characteristics of the scattering particle is the most challenging step in the implementation of the TAOS technique in particle characterization systems. The analysis performed here

explored the characteristics of the intensity islands formed in the TAOS patterns of particle aggregates as a means to distinguish between aggregates formed from different types of primary particles. The results obtained indicate that island characteristics are influenced by the composition of aerosol particle aggregate and may be useful in distinguishing between certain types of aerosol particle aggregates. This study also showed the size and number of islands found in the TAOS patterns of aggregates composed by non-penetrable objects and homogeneous rough particles were following the same variations as function of the overall particles size and surface roughness. Thus, the presence of microvoids inside the aggregates' structures does not seem to significantly modify the TAOS patterns. We believe that the results observed here can be generalized to aggregates of different dimensions, although further experiments would need to be performed in order to verify this claim. We would expect, first of all, that surface roughness effects would only be noticed for roughness scales that are commensurate with the wavelength. The results in Fig. 2 seem to indicate that aggregates with similar roughness scales (e.g. BG spores and 0.98 μm PSL) are indistinguishable so far as their island characteristics, while aggregates with different roughness scales are in general distinguishable (with various levels of success).

As evidenced in the case of BG spores and 0.98 μm PSL sphere clusters, island characteristics alone do not consist of a complete set of variables for distinction. However, with increasing processing speeds, the subset of variables extracted from applying image processing routines to TAOS patterns may be increased for better distinction power without compromising the ability to perform data analysis in real time. Moreover, the possibility of using TAOS as a complementary step to other particle interrogation techniques presents a viable option to such limitations. Indeed, we believe that hybrid approaches combining statistical sorting methods such as PCA, numerical calculations, and complimentary experimental interrogation techniques, would be the most efficient way to approach the problem of ambient aerosol characterization and detection.

References

1. Y.L. Pan, K.B. Aptowicz, R.K. Chang, M. Hart, J. Eversole, Opt. Lett. **28**, 589 (2003)
2. K.B. Aptowicz, R. Pinnick, S. Hill, Y.-L. Pan, R.K. Chang, J. Geophys. Res. **111**, D12212 (2006)
3. S. Holler, S. Zomer, G.F. Crosta, Y.L. Pan, R.K. Chang, J.R. Bottiger, Appl. Opt. **43**, 6198 (2004)
4. E. Hirst, P. Kaye, J. Geophys. Res. **101**, 19231 (1996)
5. R. Pinnick, S. Hill, P. Nachman, J. Pendleton, G. Fernandez, M. Mayo, J. Bruno, Aerosol Sci. Technol. **23**, 653 (1995)
6. S. Hill, R. Pinnick, S. Niles, Y.-L. Pan, S. Holler, R.K. Chang, J. Bottiger, B. Chen, C. Orr, G. Feather, Field Anal. Chem. Technol. **3**, 221 (1999)
7. J. Hybl, G. Lithgow, S. Buckley, Appl. Spectrosc. **57**, 1207 (2003)
8. C.F. Bohren, D.R. Huffman, *Absorption and Scattering of Light by Small Particles* (Wiley, New York, 1983)
9. J.-C. Auger, K.B. Aptowicz, R.G. Pinnick, Y.-L. Pan, R.K. Chang, Opt. Lett. **32**, 2 (2007)
10. G.E. Fernandes, Y.-L. Pan, R.K. Chang, K.B. Aptowicz, R. Pinnick, Opt. Lett. **31**, 3034 (2006)
11. J.R. Bottiger, P.J. Deluca, E.W. Stuebing, D.R. Vanreenaen, J. Aerosol Sci. **29**, 1965 (1998)
12. R.C. Gonzalez, R.E. Woods, S.L. Eddins, *Digital Image Processing Using Matlab* (Pearson Prentice Hall, Upper Saddle River, 2004)
13. K. Fukunaga, *Introduction to Statistical Pattern Recognition* (Academic Press, San Diego, 1990)
14. A. Ovcharenkoa, S. Bondarenkoa, Y. Shkuratova, C. Scotto, C. Merritt, M. Hart, J. Eversole, G. Videen, J. Quant. Spectrosc. Radiat. Transf. **101**, 462 (2006)
15. E. Zubko, Y. Shkuratov, M. Hart, J. Eversole, G. Videen, Opt. Lett. **28**, 1504 (2003)
16. S. Holler, J.C. Auger, B. Stout, Y.L. Pan, J.R. Bottiger, R.K. Chang, G. Videen, Appl. Opt. **39**, 6873 (2000)
17. J.C. Auger, B. Stout, J. Quant. Spectrosc. Radiat. Transf. **79–80**, 533 (2003)
18. M.I. Mishchenko, J.W. Hovenier, L.D. Travis, *Light Scattering by Nonspherical Particles* (Academic Press, New York, 2000)